Cement and Concrete Research 136 (2020) 106156

Contents lists available at ScienceDirect

Cement and Concrete Research

journal homepage: www.elsevier.com/locate/cemconres

Nanodispersed TiO_2 hydrosol modified Portland cement paste: The underlying role of hydration on self-cleaning mechanisms

Zixiao Wang[a,b], Qingliang Yu[b,c,*], Florent Gauvin[b], Pan Feng[a,d,**], Ran Qianping[a,d,e], H.J.H. Brouwers[b]

[a] Jiangsu Key Laboratory of Construction Materials, School of Materials Science and Engineering, Southeast University, Nanjing 211189, PR China
[b] Department of the Built Environment, Eindhoven University of Technology, 5600 MB Eindhoven, the Netherlands
[c] School of Civil Engineering, Wuhan University, 430072 Wuhan, PR China
[d] State Key Laboratory of High Performance Civil Engineering Materials, Nanjing 210008, PR China
[e] Jiangsu Research Institute of Building Science, Nanjing, Jiangsu 210008, PR China

ARTICLE INFO

Keywords:
Nanodispersed TiO_2 hydrosol
Self-cleaning performance
Optical parameters
Portland cement
Hydration

ABSTRACT

The self-cleaning performance of photocatalytic cement paste is related to the dispersion of nano-TiO_2 in the hardened matrix. This work aims to study the influences of Portland cement hydration on the self-cleaning behaviour of acidic anatase TiO_2 hydrosol modified hardened Portland cement paste (HPCP), and the working mechanisms. The presence of TiO_2 hydrosol results in the retardation of hydration at early age and better self-cleaning performance of HPCP. The additional surface defects of TiO_2 in HPCP are the main reason of self-cleaning performance enhancement. The morphology and the pore size distribution of hydration products also contribute to the enhancement of self-cleaning performance by the surface electron capture effect, which are supported by the analyses of Confocal Raman Microscopy and Scanning Electron Microscope. A new mechanism is suggested to explain the role of photocatalytic property and cement hydration on the enhancement of self-cleaning performance of HPCP with different concentration of TiO_2 hydrosol.

1. Introduction

Cementitious materials, especially those exposed to outdoor conditions, are directly and continuously exposed to many pollutants (e.g. organic, inorganic and particulate matter) and microorganisms under different weather. These pollutants can aggravate the deterioration process of concrete structures and cause important changes in the materials properties, like aesthetic and physical properties degradation [1,2]. Nano TiO_2-based photocatalysis has proved to be a promising technology for the efficient degradation of a range of organic compounds (e.g. volatile organic compounds) and inorganic compounds (e.g. NO_X and SO_2), in busy canyon streets [3,4], road tunnels and urban environments [5], etc.

Due to the different synthesis process, nanodispersed TiO_2 hydrosol [6–10] and TiO_2 nano- powder [11–14] present different agglomeration morphology and surface charge distribution in aqueous solutions. In general, the TiO_2 particles in hydrosol are positively charged and the hydrodynamic diameter is < 100 nm [6,9,15–18]. Though the crystal size of TiO_2 particles in nano powder is in nano scale, it is difficult to obtain the nano dispersed TiO_2 suspension by re-dispersing nano powders in water [19]. Moreover, the surface charge of nano TiO_2 is influenced by the pH of system. According to several studies, the isoelectric point of TiO_2 nano powders [20–23] and hydrosols [9,24] varies in the pH range of 5–6.8, meaning the positively charged TiO_2 nano particles will become negatively charged when the pH is higher than the isoelectric point. As to the strong ionic alkaline system of cement-based materials, the surface charge and agglomeration behaviours of nano TiO_2 should be influenced in theory. In addition, cement hydration involves a collection of coupled chemical processes of dissolution, diffusion, growth, nucleation, complexation and adsorption, each of which occurs at a rate that is determined both by the nature of the process and by the state of the system at that instant [25]. Based on the

* Correspondence to: Q. Yu, Department of the Built Environment, Eindhoven University of Technology, 5600 MB Eindhoven, the Netherlands.
** Correspondence to: P. Feng, Jiangsu Key Laboratory of Construction Materials, School of Materials Science and Engineering, Southeast University, Nanjing 211189, PR China.
E-mail addresses: q.yu@bwk.tue.nl (Q. Yu), pan.feng@seu.edu.cn (P. Feng).

https://doi.org/10.1016/j.cemconres.2020.106156
Received 8 November 2019; Received in revised form 2 June 2020; Accepted 7 June 2020

Table 1
The physical and chemical parameters of nano TiO_2.

	Hydrodynamic size ± SD (d. nm)	Zeta potential (mV)	Polydispersity Index	Crystal pattern	BET specific surface area (m^2/g)	Absorption average pore width(nm)
Hydrosol	18.92 ± 6.358	43.4	0.114	–	–	–
Xerogel	–	–	–	Pure anatase	244.75	5.76

previous studies [26–30], the nano TiO_2 powders are often understood as accelerating the cement hydration because of the filler effect or nucleation effect. Since the TiO_2 particles are positively charged in hydrosol and negatively charged in water suspensions made of nano powders, there may exist different factors that can influence the hydration process of cement, particularly at early age. Moreover, due to the inorganic or organic acids being selected as the peptizators in the synthesis process of TiO_2 hydrosol [9], the catalogue of surface banded functional groups might be influenced by the different peptizators, which might also influence the cement hydration process.

The dispersion of nano TiO_2 and the aggregation morphology affected by cement hydration products on the surface of hardened cement paste is the key factor to the self-cleaning performance of the modified cement paste. Many studies [31–36] have investigated photocatalytic and self-cleaning performances, mechanic properties and durability of cementitious materials modified by nano TiO_2 powders in relatively large dosages. Most results reveal that typically w.t. 3%- 5% of TiO_2 nano powders (of cement) modified cement-based material presents satisfying photocatalytic performance, indicating the lower concentration of TiO_2 nano powders cannot have good photocatalytic performance in cementitious materials. These may be caused by the faster recombination of photo excited electrons and holes on the surfaces of agglomerated TiO_2 particles [37]. Unlike the TiO_2 nano powders, TiO_2 hydrosol catalysts can be easily separated, collected and re-dispersed for continuous reuse because of its sensitivity to pH value and electrolyte strength of medium [15–18,21,22]. Some research results show that nanodispersed TiO_2 hydrosols exhibit high photochemical reactivity, even superior to nano TiO_2 powders in aqueous environment [7,10]. The stable TiO_2 hydrosols have the great specific surface areas and high photocatalytic property, which have been used to prepare coatings [7,38]. The preparation of cement paste is the reaction between water and cement clinkers, and the TiO_2 hydrosol can be blended into water, like superplasticizers, without agglomeration, which means nano TiO_2 particles via hydrosols may be easily and well dispersed in cement paste matrices.

Some studies [39,40] suggested hypotheses of self-cleaning mechanism concerning TiO_2 nano powders modified mortar, for example the chemical composition of cement seems to prevail over the effect of the optical parameters and electronic band structure for mortar made of slag cement; the final microstructure of the material influenced the photocatalytic property of mortar. The research on the self-cleaning performance of TiO_2 hydrosol modified Portland cement paste is also rare, let alone explaining the self-cleaning mechanism of TiO_2 hydrosol in hardened cement paste [41]. Moreover, because of the potential concerns about the negative effects of low pH induced by the TiO_2 hydrosol, few works have studied the effects of the surface charge and surface functional group of nano TiO_2 on the Portland cement hydration process.

This work aims to study the influences of surface bonded functional groups of TiO_2 hydrosol on cement hydration process, and the self-cleaning performance of cement paste modified by nano dispersed TiO_2 hydrosol in very low dosages, measured at different hydration ages. The possible self-cleaning enhancement mechanism of TiO_2 hydrosol modified cement paste are suggested in the view of semiconductor properties of TiO_2 in hardened cement paste and morphology of cement hydration products.

2. Experimental

2.1. Materials

2.1.1. Nano dispersed TiO_2 hydrosol

TiO_2 hydrosols are synthesized based on the precipitation-peptization methods [42] but at the lower temperature (40 °C), because the TiO_2 hydrosol presents smaller hydrodynamic particles size synthesized at lower temperatures [6]. Titanium tetra-isopropoxide (TTIP, 97.0%) purchased from Sigma-Aldrich. Acetic acid glacial (CH_3COOH, 99.6%) and absolute ethanol (C_2H_5OH, 99.9%) purchased from VWR Chemicals, and deionized water (18.2 MΩ.cm) are used in the preparation process. The physical and chemical parameters of synthesized TiO_2 hydrosol are listed in Table 1. To evaluate the crystal type and specific surface area of TiO_2, the TiO_2 xerogel is made by drying hydrosol with unhindered shrinkage at 105 °C for 24 h.

2.1.2. Sample preparation

CEM I 52.5 R cement and tap water are used to prepare the cement paste. The water to cement mass ratio is 0.4. The samples are wet mixed for 4 min before moulded in 4 cm × 4 cm × 4 cm moulds and covered with plastic sheet. Different amounts of TiO_2 hydrosol are mixed in mixing-water before added into the cement. The TiO_2 to cement mass ratios are 0%, 0.01%, 0.05% and 0.10%, respectively. After 1 day of curing, the samples are demoulded and cured in the climate chamber (RH > 95%, 20 °C) until the test ages.

2.2. Methods

2.2.1. Particle size and zeta potential evaluation

The TiO_2 hydrosol samples are tested three times by a Zetasizer Nano Series (Malvern Panalytical, United Kingdom) applying the dynamic light scattering (DLS) principle. The basic distribution of particle size obtained from a DLS measurement is intensity. The Zetasizer Nano Series calculates the zeta potential by determining the electrophoretic mobility and then applying the Henry equation. The electrophoretic mobility is obtained by performing an electrophoresis experiment to the sample and measuring the velocity of the particles using laser Doppler velocimetry. Prior to the test, the initial hydrosol is diluted in distilled water for 100 times.

2.2.2. Hydration heat measurement

The calorimetry test is performed using an isothermal calorimeter (TAM Air, TA Instruments, United States) at 20 °C. Cement is firstly mixed with distilled water and TiO_2 hydrosol, then the resulting paste is injected into an ampoule that is then sealed by a lid and loaded into the calorimeter. The heat flow is recorded for 140 h.

2.2.3. X-ray diffraction pattern

The phase compositions of TiO_2 xerogel and TiO_2 modified cement paste samples are investigated by comparing X-ray diffraction (XRD) pattern (Bruker D4 PHASER, Philips, The Netherlands) with a Co tube (40 kV, 40 mA). A typical run is made with a step size of 0.02°/min and a dwell time of 0.5 s.

2.2.4. Spectral analysis

ATR-FTIR is used to analyse the functional groups around the

surface of the TiO_2 particles in hydrosol. A Fourier-transform infrared spectroscopy (FTIR) spectrometer (PerkinElmer, United States) equipped with an attenuated total reflectance (ATR) accessory (GladiATR, PIKE technologies, United States) is used here. Liquid samples are dropped evenly onto the surface of the ATR Ge crystal, and the FTIR spectra are recorded from 400 to 4000 cm^{-1} at a resolution of 4 cm^{-1} by 32 scans. For each scanning, the spectrum is collected by subtracting the original spectrum from the air background spectrum. Then, the obtained spectra are baseline corrected.

The reflectance spectra of TiO_2 modified hardened cement paste samples at 28 days are measured by the UV-VIS-NIR spectrophotometer (Perkin Elmer Lambda 750), the tested range is 200 nm to 800 nm, 2 nm per second. To meet the test requirement, the paste samples are cut into slices with the thickness of 1 cm.

The distribution of phases at the surface of hardened cement paste at 28 days is observed by Confocal Raman Microscopy (Witec alpha300S, Witec, Ulm, Germany). Raman spectra are recorded over a spectral range from 0 cm^{-1} to 3900 cm^{-1}. Confocal Raman measurements are accomplished using a 532.306 nm excitation laser with the power of 30.159 mW. The scan area is 20 μm × 20 μm, the size of the Raman images is 20 × 20 pixels with the integration time per pixel of 2 s. The collected Raman spectra are analysed by using WITec Suite 5.2 software (Witec, Ulm, Germany). For the process of the results obtained by CRM, 'cosmic ray removal' and 'background subtraction' are performed.

2.2.5. Thermal-gravimetric analysis

The thermal-gravimetric (TG) analysis is conducted using a STA 449 F1 instrument, cement paste samples are heated up to 1000 °C from 40 °C at the rate of 10 °C/min with nitrogen as the carrier gas. Before the test, samples at the age of 1 day, 3 days, 14 days and 28 days are crushed and immersed in acetone for 7 days and then dried in the oven at 40 °C to cease the further hydration.

2.2.6. Nitrogen adsorption/desorption (NAD) test

In this study, the Brunauer, Emmett and Teller (BET) method, which is the mostly used method to deduce the internal specific area of pores based on the multi-molecular adsorption assumptions, is used to measure the specific surface area of cement paste containing different dosages of TiO_2 hydrosols. The pore size distribution from the adsorption isotherm was evaluated by the Barrett-Joyner-Halenda (BJH) interpretation. Nitrogen sorption isotherm experiments are carried out at 77 K temperature by a NAD device of type TriStar II 3020 with the nitrogen pressure range up to 950 mmHg and the measurement range of the specific surface area is from 0.01 m^2/g, nitrogen unit. The cement paste samples at 1 day and 28 days are dried at 40 °C and degassed in an external degassing station at 40 °C under N_2 flow for 4 h. In these degasing conditions, the microstructure of early hydration products in the cement pastes is not affected.

2.2.7. Scanning electron microscope (SEM) analysis

The cement paste samples are prepared based on the process described in Section 2.1. The paste samples are cut into thin slices at 1 day and 28 days, and the hydration of the samples for SEM tests is ceased for the further hydration. Before the tests, all the samples are sputtered by gold for enhancing the electrical conductivity. In order to obtain the microstructure of the samples with different concentrations of TiO_2 hydrosols, micrographs are recorded by using a Quanta 250 FEG scanning electron microscope (ThermoFisher scientific, USA) with secondary electrons detector at an accelerating voltage of 15 kV.

2.2.8. Self-cleaning performance characterization

Rhodamine B(RB) is an organic dye, the chromophoric group of which has the maximum lightweight absorption at about 554 nm [43]. Normally, the RB water solution presents the colour of red to violet red, and the dried RB film on solid materials also presents the same colour. Since the chromophoric group of RB molecules can be destroyed by in the photo-degrading process [44,45], the colour change of dried RB film on the surface of hardened cement paste can be used to interpret its degradation. In this study, the self-cleaning ability of the TiO_2 hydrosol modified HPCP is evaluated by colorimetric analysis of the degradation of Rhodamine B (RB).

Before tests, the paste top surfaces are polished by SiC sandpapers to obtain a relatively smooth surface with the roughness in the range of 10 to 14 μm. Each surface area of paste sample is stained by painting 600 μL of 0.1 mM RB aqueous solution. Then the samples are kept overnight in dark at room temperature for drying. For each coated specimen, 9 points are tested for the colorimetric tests and each point is tested 4 times. The samples are exposed to a UV lamp (10 ± 0.05 W/m^2) to simulate UV light in natural conditions, and the discoloration of the stains is monitored.

The reflected colour measurements are taken directly on the surface of each point on each sample at different illumination time with a spectrometer (USB4000, Ocean optics, United Kingdom), which is optimized for the 380–780 nm wavelength range and analysed mathematically to yield colorimetric quantities like xyz, RGB or L*a*b*. In this study, the percentage of discoloration is expressed with the coordinate of the dominant colour of dye a*, value of the CIE Lab colour space for RB [34,35] [46], according to:

$$\%\text{colour change} = \frac{a_0^* - a_t^*}{a_0^*} \times 100 \quad (1)$$

Where, a_0^* is the value of a* at time 0 before irradiation, a_t^* is the value after t minutes irradiation.

3. Results

3.1. Dispersion and surface functional group of TiO_2 in hydrosol

Fig. 1 presents the ATR-FTIR spectra of the TiO_2 hydrosol and xerogel. The measured solid content of TiO_2 particles in hydrosol is about 1.54%, the majority parts in hydrosol are water and acetic acid. As the red curve shown in Fig. 2, the main absorbance peaks are –OH of water and $–COO^-$ and –C–OH of acetic acid, the typical peaks of TiO_2 are covered by those strong peaks. So, the spectrum of TiO_2 xerogel reflected the functional groups on the nano TiO_2 particles much clearer. As the black curve shown in Fig. 2, the strong C=O peak near 1527 cm^{-1} [47,48] of TiO_2 xerogel is assigned to carboxyl groups on the surface of TiO_2, resulting from the acetic acid used in the peptization process [7]. The appearance of vibrations around 1440 cm^{-1} in the

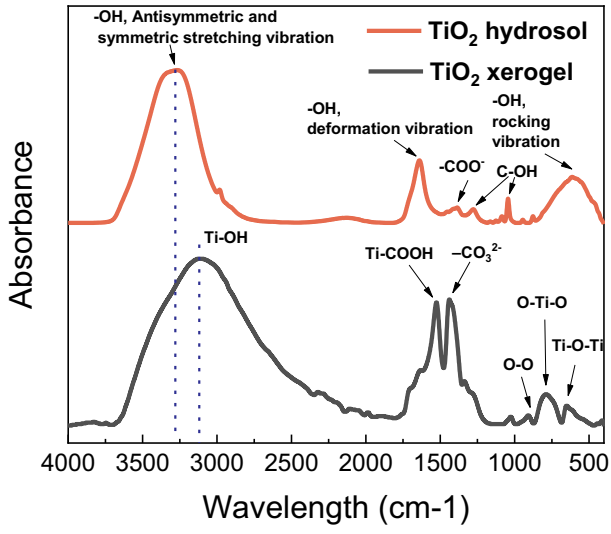

Fig. 1. The FTIR absorbance spectra of TiO_2 hydrosol and dried xerogel.

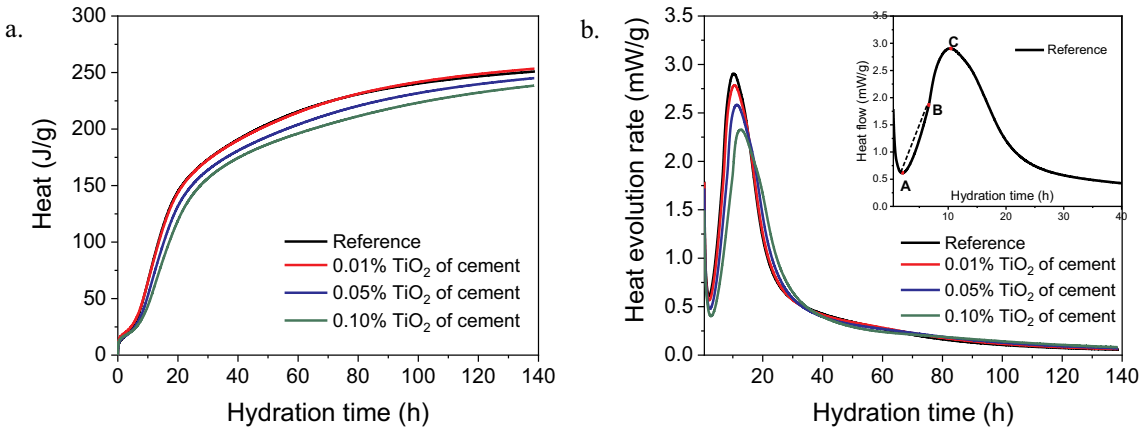

Fig. 2. Influence of different concentration of TiO_2 hydrosol on the exothermic heat flow per mass of binder and total heat of cement paste.

fresh xerogel suggested a substantial surface coverage of $-CO_3^{2-}$ resulting from the reaction of carbonation during the drying process [49]. The strong wide peak near 3500–2800 cm^{-1} is due to the stretching vibration of –OH group, which represented the OH groups on the surface of TiO_2 [7]. The peaks corresponding to O—O, O–Ti–O and Ti–O–Ti bonds are identified at 912 cm^{-1}, 794 cm^{-1} and 655 cm^{-1} [49,50]. These results indicated that sufficient hydroxyl groups like –OH and –COOH are absorbed on the surface of TiO_2 nanoparticles. It is seen that in TiO_2 hydrosol, the TiO_2 particles are positively charged and surface absorbed by –OH and –COOH via chemisorption, which is negatively charged in suspension by re-dispersing nano TiO_2 powder in solution at neutral or higher pH because of the absorption of O^- and –OH [51,52]. The absorption of –COOH makes the TiO_2 hydrosol different from the suspension made of nano TiO_2 powders. When mixing this TiO_2 hydrosol into cement paste, the hydration process might be influenced because of the different surface functional groups and charges, which will be discussed in the next section.

3.2. Effects of TiO_2 hydrosol on cement hydration

3.2.1. Hydration heat

The cumulative heat release and rate of hydration of cement paste containing TiO_2 hydrosol are shown in Fig. 2. Fig. 2 (a) indicates that the total hydration heat remained similar as the TiO_2 dosage is 0.01% and beyond that dosage the hydration heat decreased with the increase of TiO_2 amount. As can be seen from Fig. 2 (b), after mixing with TiO_2 hydrosols, the hydration rate decreases and the descent scope is greater as the dosage of TiO_2 increased. Meanwhile, the time of occurrence of heat flow peaks in the blank and TiO_2 modified cement is different, and a delay is observed when TiO_2 hydrosol is used in the cement paste. The retardation of that exothermic peak is greater with the increase content of TiO_2.

To analyse the influences of TiO_2 hydrosol on the hydration kinetics in detail, six parameters are calculated from the heat evolution curves in Fig. 2, see the illustration shown in the detailed view of the heat evolution curve of the reference sample in Fig. 2(b). The obtained hydration parameters are listed in Table 2. The hydration rate in the induction period and the duration of the induction period t_A [53] are related to the diffusion rate of various ions from the mineral phases to the aqueous phase [25,54,55]. The ions diffusion rates are mainly dominated by the contact surface between the mineral grains and water. In Table 2, the ending time point of the induction period (t_A) of cement hydration is delayed due to the presence of TiO_2 hydrosol, and the retardation increased with the concentration of TiO_2 hydrosol in cement paste. Adding 0.05% and 0.10% TiO_2 hydrosol evidently prolongs the induction period and depresses the hydration rate $(dQ/dt)_A$ in the induction period, implying the decelerated ion diffusion causes by the prominent adsorption of TiO_2 particles on cement surface. The slight influences on the heat evolution parameters of cement hydration are found when 0.01% TiO_2 hydrosol is added, which is because of the low amount of adsorption functional groups on cement grains surfaces.

Table 2
Parameters of cement hydration extracted from the calorimetry curves of the reference cement paste and the cement pastes containing different concentration of TiO_2 hydrosol.

Item	t_A (h)	$(dQ/dt)_A$ (mW/g)	Q_A (J/g)	t_C (h)	$(dQ/dt)_C$ (mW/g)	Q_C (J/g)	K_{A-B} (mW/(g·h))	Q_{A-C} (J/g)
Reference	2.06	0.61	17.19	10.34	2.91	68.56	0.26	51.37
0.01%	2.12	0.57	19.33	10.52	2.78	69.83	0.24	50.50
0.05%	2.36	0.48	16.67	11.35	2.58	65.08	0.22	48.42
0.10%	2.78	0.40	17.94	12.67	2.33	64.80	0.21	46.86

t_A: the ending time point of the induction period.
t_C: the time point of the maximum heat generation rate.
t_B: the inflection point between A and C on the heat evolution curve, refers to the time point of the maximum acceleration rate.
$(dQ/dt)_A$: the heat generation rate during the induction period, the cumulative heat flow at the beginning of the acceleration period Q_A.
$(dQ/dt)_C$: the maximum hydration rate in the acceleration period.
Q_{A-C}: the cumulative heat flow during the acceleration period.
K_{A-B}: The secant slope on the heat evolution curve between A and B, which represents the acceleration rate of hydration rate at the early stage of the acceleration period.

After the induction period, cement hydration steps into the acceleration period with rapid nucleation and growth of hydrates. The hydration rate in the acceleration period is determined by the total amount of hydrate nuclei of C-S-H [55–57]. Thus, K_{A-B} reflects the nucleation rate of C–S–H at the early stage of the acceleration period. In Table 2, K_{A-B} and $(dQ/dt)_C$ visibly drop with the concentration of TiO_2 hydrosol, suggesting that TiO_2 depresses the nucleation of hydrates during the acceleration period, which may be ascribed to the absorbance of TiO_2 particles with calcium. As described in Section 3.1, the –COOH, –OH and $-CO_3^{2-}$ are observed on the surface of TiO_2 xerogel and TiO_2 particles in hydrosol. The measured zeta potential of TiO_2 hydrosol is positive, indicating the positive charge of functional groups ($-OH_2^+$ [51,52]) played a dominant role on the surface of TiO_2 particles in acidic solution. While in cement pore solution with very high pH, the surface of TiO_2 nano particles turns into negative because the solution pH is higher than the isoelectric point (in a pH range of 5.6–6.0 [21,58]). The TiO_2 particles can absorb on the surfaces of positively charged cement grains that hinder the exchange of water and ions and poison the nucleation sites.

With the growth of hydration products, a hydrate layer is gradually formed over the surfaces of cement grains, which further hinders the

exchange of water and the ions and then advances to the deceleration period of cement hydration (diffusion-controlled reaction) at time point t_C. The maximum hydration rate is mainly determined by the number of nuclei formed during the time periods A to C. The lower hydration peak is related to fewer nuclei existing during A to C. Thus, from the lower hydration peak $(dQ/dt)_C$, it can be deducted that the total nuclei number is reduced when more TiO_2 hydrosol is added into cement paste. In addition, the higher concentration of TiO_2 hydrosol decreases the cumulative heat flow Q_{A-C} during the acceleration period, which is due to the decrease of nuclei during point A to point C. These results revealed TiO_2 hydrosol prolonged the induction period, delayed the hydration peak due to the absorption on cement surface, and a higher concentration of TiO_2 indicated a larger absorption amount. The high adsorption of TiO_2 reduced the diffusion rate of ions and water transporting to the interface between the cement and aqueous phases, consequently depressed the nucleation process of cement hydration. These retardation effects of nano dispersed TiO_2 hydrosol on cement hydration are similar to the retardation effect of polycarboxylate salts on cement hydration. Compared with the polycarboxylate salts, like polycarboxylate based superplasticizers or polymers, the retardation effect is not significant because the isolated carboxyl groups on TiO_2 surfaces are less effective for retardation of cement hydration compared with triad, tetrad, pentad, etc. [53,59,60].

3.2.2. Hydration products

The XRD patterns of cement with different concentrations of TiO_2 at 1 day and 28 days are shown in Fig. 3. The reference and TiO_2 modified samples presented similar mineral compositions and hydration products, the main clinkers are C_3S, C_2S, C_3A and C_4AF, and the main hydration products are CH, C-S-H and AFt, which meant the kinds of hydration products are not influenced by the TiO_2 hydrosol.

The TGA curves of cement pastes can be divided into two major parts, representing three different kinds of reactions [61–63]: (1) 105 °C to 300 °C: the primary range of dehydration of C-S-H gel. (2) 400 °C to 500 °C: dehydroxylation of calcium hydroxide (CH). (3) 600 °C to 800 °C: decarbonation of calcium carbonate. According to the suggested calculation method in literature [61,64,65], the CH and non-evaporation water in cement paste samples measured by TGA are shown in Table 3. Both CH and non-evaporable water are expressed as a percentage of weight of the dried paste samples. In Table 3, the CH contents in paste mixed with TiO_2 at the age of 1 day decreases with the concentration of TiO_2 hydrosol, indicating the cement hydration is retarded. At 28 days, the CH contents in the paste containing TiO_2 are very close to the reference cement paste. These results indicated that the presence of TiO_2 hydrosol had delayed the hydration of clinker grains at early age but had insignificant influence on the hydration at later stage.

Based on the analysis of hydration heat, XRD pattern and thermal decomposition behaviour of cement paste, it can be confirmed that the chemical reactions during the cement hydration process have been altered with the introduction of TiO_2 hydrosols, by consuming portlandite crystals and influencing the contents of hydration products. For further analysing the influence of TiO_2 hydrosol on the hardened cement paste, the specific surface, pore size distribution and SEM images of hardened cement paste will be discussed in Section 3.4.

3.3. Self-cleaning performance and optical parameters determination

3.3.1. Self-cleaning performance

The percentage of colour change for a* for RB caused by the self-cleaning effect of TiO_2 containing cement paste is presented in Fig. 4. The colour change of samples containing TiO_2 increases quickly during the first 6 h irradiation, the differences between TiO_2 hydrosol contents are significant. In addition, the colour change of the samples' surfaces is also influenced by the hydration ages of cement, as shown in Fig. 4. At early age, for example 7 days, the sample containing 0.05% and 0.10% nano TiO_2 are very close in self-cleaning performance, and the highest colour change rate (60.15%, 0.10% TiO_2) is obtained after 44 h irradiation. Moreover, compared with the control cement paste sample, the paste containing 0.01% TiO_2 at 7 days shows a certain self-cleaning property, the colour change rate is 21.47% after 44 h UV irradiation. Because the cement hydration is not completely in the paste samples, the surface colour change of the samples is influenced by the colour change of cement matrix at 7 days and 14 days, and the colour change rates are negative at the first 2 h UV irradiation. At 28 days, the tested data at first 2 h are much more stable. The colour change rate of sample surfaces increases with the increased concentration of TiO_2 hydrosol, namely the colour change rates are 35.3%, 49.0% and 53.4% after 44 h UV irradiation with 0.01%, 0.05% and 0.10% TiO_2 hydrosol, respectively.

According to the previous studies [44,45,66,67], the maximum absorbance band of RB in the visible light range is about 554 nm, which is the typical absorbance peak of chromophoric groups of RB. To eliminate the interference of the light absorbance of cement paste matrix, the absorbance spectra of baseline at the range of 400 to 800 nm are removed from HPCP samples contains 0.05% TiO_2, which are tested at three curing ages under different duration of UV irradiation, as shown in Fig. 5. The full information of the absorbance spectra curves with and without baselines of each tested HPCP samples are presented in the Fig. S1 and Fig. S2 in the supplementary material. For further clarification, several photos of the surface colour of HPCP samples after 44 h of UV irradiation are shown in Table S1 in the supplementary material. The peak positions of absorbance spectra before and after 44 h of UV irradiation are marked in Fig. 5. After 7 days

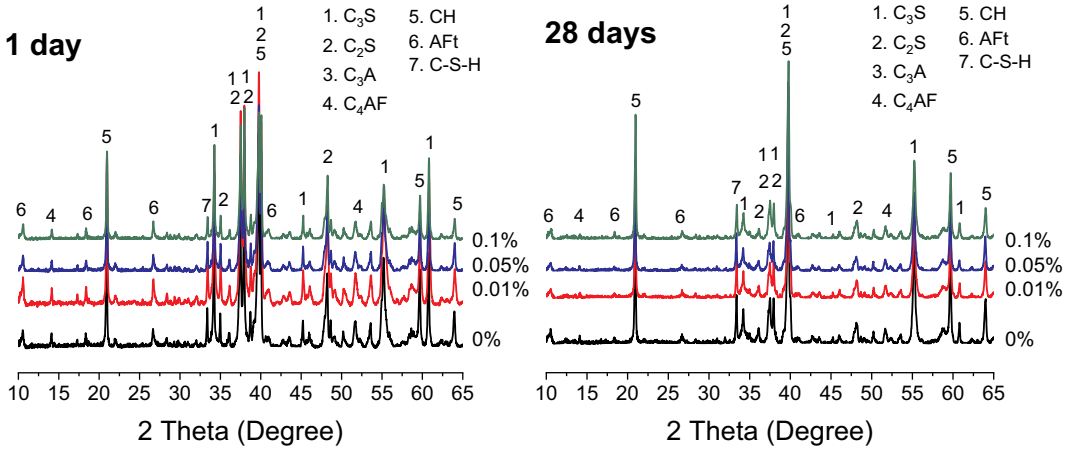

Fig. 3. The XRD pattern spectra of cement paste containing different amount of TiO_2 hydrosol at 1 day and 28 days.

Table 3
Non-evaporable water and $Ca(OH)_2$ content of hydrated cements.

Dosage of TiO_2	Non-evaporable water (%)				$Ca(OH)_2$ (%)			
	1 d	3 d	14 d	28 d	1 d	3 d	14 d	28 d
0%TiO_2	11.19	14.82	15.49	17.19	16.61	22.10	22.83	23.22
0.01%TiO_2	11.16	14.57	16.77	17.75	16.45	21.90	21.55	22.24
0.05%TiO_2	11.12	14.56	17.42	18.16	16.23	21.74	21.68	22.51
0.10%TiO_2	9.62	14.79	17.56	17.19	14.86	20.53	22.39	22.92

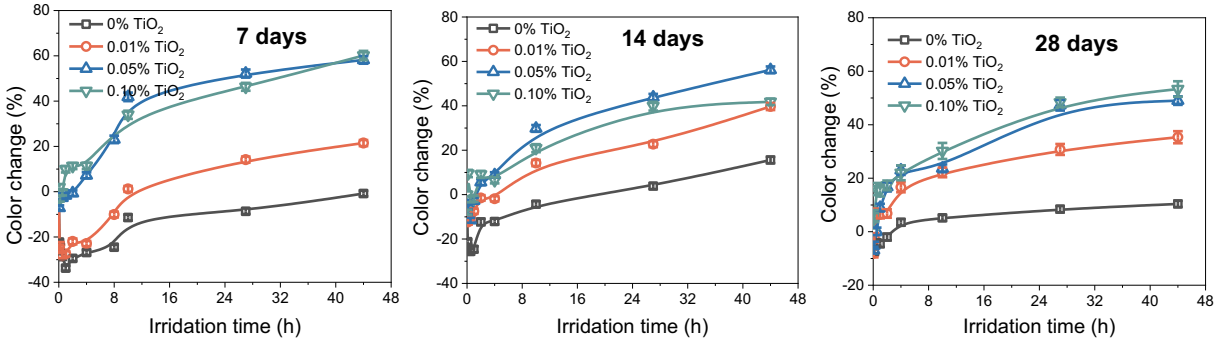

Fig. 4. Percentage of colour change rate of a* for RB on the surface of hardened cement paste with different concentration of TiO_2 at different ages.

and 14 days curing, in all TiO_2 hydrosol modified HPCP, the absorbance at 554 nm increases in the first 0.5 to 2 h of UV irradiation, then decreases in the rest of UV irradiation duration. The variation of peak values at 554 nm presents the similar changing trend as the variation of surface colour shown in Fig. 4, which confirms that the colour change of RB on the surface of mortar is caused by photo-bleaching [44]. Although the slow photobleaching of RB in air can still be observed under visible light, it can be seen from Fig. 4 and Fig. 5 that the presence of TiO_2 hydrosol in mortar has promoted the photobleaching effect on the degradation of RB. In Fig. 5, another obvious phenomenon, the so called peak hypsochromic shift (or blue shift), is also observed in HPCP modified by TiO_2 hydrosol. It has been previously reported that the blue shift in the maximum absorption of RB water solution and dried RB film on the surface of mortar is induced by the N-deethylation of RB molecules [44,45,68], which is a significant indicator of photocatalytic degradation of RB by photocatalysts. It's noted that these two degradation processes are different processes in the primary steps of the photo-degradation of RB. The decrease of peak value refers to the photo-bleaching process, while the blue shift value refers to the N-deethylation process. As a result, for HPCP modified by a lower content (< 0.05%) of TiO_2 hydrosol, the weight of N-deethylation process increases with the age of cement paste. While, for the HPCP modified by a higher content (> 0.05%) of TiO_2, the maximum weight of the N-deethylation process appears at the age of 14 days. It is concluded that the degradation of dried RB film on the surface of HPCP goes via both the photo-bleaching process and N-deethylation process, which are both influenced by the age of the cement paste and the concentration of TiO_2 in the paste. In other words, the weight of the photo-bleaching and N-deethylation processes could be directed by designing the mix proportion of TiO_2 hydrosol modified cement paste.

Table 4 summarises some results of self-cleaning performance of photocatalytic cement paste or mortar in literatures. Compared with the RB degradation rate in Table 4, the tested TiO_2 hydrosol presents good self-cleaning performance at such low concentration in hardened cement paste. Thus, an excellent self-cleaning performance of samples is yielded by adding such low dosages of TiO_2 hydrosols in the mixing water.

However, it is observed that the colour change rate of hardened cement paste at higher concentration, for example 0.05%, reduced with the increase of hydration age. Moreover, the colour change rate induced by 0.05% TiO_2 is close to that induced by 0.10% TiO_2, indicating the self-cleaning performance of hardened cement paste does not increase proportionally with the concentration increase of TiO_2 in matrix at higher contents. Particularly, at 28 days, the self-cleaning performance of samples containing 0.10% TiO_2 is only slightly better than that of samples containing 0.05% TiO_2, revealing the cement hydration products affect the self-cleaning performance. As discussed in Section 3.2, the hydration rate and hydration products amounts are influenced by the mixing with TiO_2 hydrosol, in other words, the microstructure of the hardened cement paste samples modified by TiO_2 hydrosol is

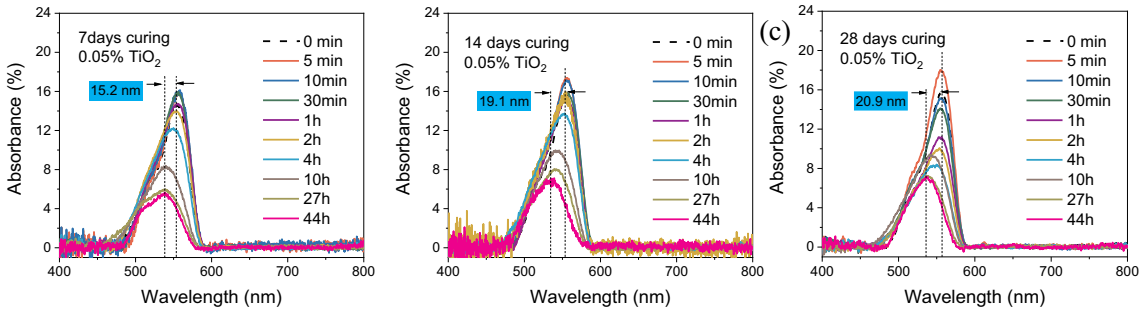

Fig. 5. The absorbance spectra curves with the baseline removed of HPCP modified by 0.05% TiO_2 at different curing age under UV irradiation during UV irradiation, (a, b, c) are spectra of the HPCP with 0.05% TiO_2 tested at 7, 14, and 28 days.

Table 4
The self-cleaning performance of nano TiO_2 (RB degradation rate) reported in literatures.

TiO_2 type	TiO_2 wt% of cement	Sample	Water to binder rate	UV density (W/m^2)	About 4 h degradation (%)	About 24 h degradation (%)	Literature
Nano powder	2	Mortar	0.5	10	35	60	[40]
	5	Paste	0.48	0.4	15	25	[32]
	2% suspension + 3% powder	Mortar	0.5	10	40	56	[35]
Hydrosol	0.1	Paste	0.4	10	22	48	This study

different from the reference paste at the same hydration age. From the view of the compound photocatalyst, the optical parameters of TiO_2-Cement paste can explain the self-cleaning ability of TiO_2 modified paste, which will be discussed in the Section 3.3.2.

3.3.2. Optical band energy and Urbach energy determination

The properties UV-VIS reflectance of hardened cement paste samples containing different concentration of TiO_2 at 28 days are measured. In order to obtain the band energy (E_g) of TiO_2 modified cement paste samples, the Kubelka-Munk optical absorption coefficient F(R) is first calculated. F(R) and E_g are calculated using the Eq. (2) and the Tauc's relation in Eq. (3).

$$F(R) = (1 - R)^2/2R \tag{2}$$

$$F(R)h\upsilon = (h\upsilon - E_g)^n \tag{3}$$

where, R is the reflectance of TiO_2-Cement paste compound; n is the exponent that depends on the type of transition, h is the Planck constant, and υ is the photon's frequency. $n = 2$ for indirect allowed transitions, and $n = 1/2$ for direct allowed transitions. As to TiO_2 photocatalyst, the modified Kubelka-Munk function with n = 2 is used in some reports [69,70]. The band energy E_g is derived from the intercept of this straight line with the photon energy axis at F(R) = 0 [71] (Fig. 6(a)).

Fig. 6(a) shows the Tauc's plot of the TiO_2 modified hardened cement paste samples. The optical energy band edges of TiO_2 modified cement paste slightly decreases with the concentration of TiO_2 as shown in Table 5. The lowering of band edge in TiO_2 modified samples can be caused by the existence of localized defect states in the forbidden zone of TiO_2-photocatalyst near the bottom/top of its conduction/valence band [39]. This result reflects the fact that the hardened cement paste matrix might disturb the semiconductor electronic structure of semiconductor through the creation of defects [39,72].

Moreover, this distortion can bring an Urbach type absorption which occurs due to the electron transition between extended band and localized band tail. The structural disorder caused by impurities and defects (Ti^{3+} and oxygen vacancies) produce an absorption tail extending deep into the forbidden gap. This absorption tail is called

Table 5
Band energy and Urbach energy of TiO_2 modified hardened cement pastes.

TiO_2 concentration	Band energy (eV)	Urbach energy(eV)
0.01%	2.79	2.98
0.05%	2.74	3.20
0.10%	2.71	2.54

Urbach tail and the associated energy is named Urbach energy (E_u), which is the width of the tails states in the bandgap associated with the structural defects and disorder within the crystal. The linear region (exponential tail) is the direct manifestation of the presence of structural defects in the crystal, which results in formation of band tail states below (above) the conduction (valence) band and their density of states falls sharply with energy [73]. The exponential character of the absorption coefficient near the absorption edge is expressed by the Urbach rule [74,75], which is given by.

$$F(R) = k\ \exp(h\upsilon/E_u) \tag{4}$$

$$\ln\ F(R) = \frac{1}{E_u}h\upsilon + \ln\ k \tag{5}$$

where k is a characteristic crystal constant, hυ is the incident photon energy, and E_u is the Urbach energy, F(R) is the Kubelka-Munk optical absorption coefficient mentioned before.

Fig. 6(b) presents the Urbach energy of TiO_2 modified hardened cement paste samples. The fitting lines of the absorption data near band edge showed that the absorption edge followed the Urbach tail behaviour indeed. The E_u of TiO_2 modified cement paste increased when the TiO_2 concentration increases from 0.01% to 0.05%, and then decreased when the TiO_2 concentration is 0.10%. The increase of E_u meant the presence of additional structural or crystalline defects like low angle grain boundaries, additional growth sites on the surface, disorder, oxygen vacancies etc. [73].

The results of Urbach energy indicated the hardened cement paste containing 0.05% TiO_2 presents the highest photocatalytic activity, theoretically the self-cleaning performance of that compound is supposed to be the best in the tested samples. Since the cement paste is a

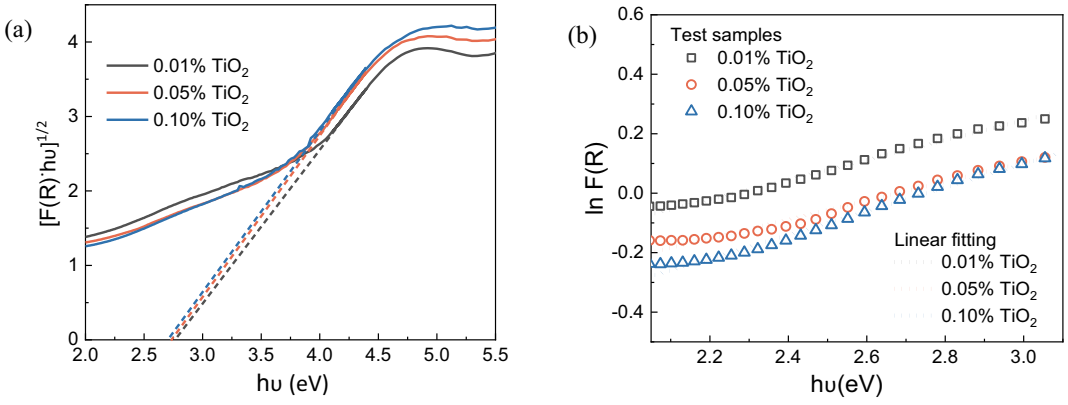

Fig. 6. Tauc's plots and determination of Urbach energy of the hardened cement pastes.

Table 6
BET surface area of cement paste.

TiO_2: cement	Age (d)	BET SSA (m^2/g)	Adsorption average pore width (nm)	Decrease rate of BET SSA (%)	Decrease rate of adsorption average pore width (%)
0%	1	17.06	20.64	55.74	24.76
	28	7.55	15.53		
0.01%	1	15.11	21.87	61.95	31.24
	28	6.52	15.04		
0.05%	1	15.02	21.18	33.49	37.96
	28	9.99	13.14		
0.10%	1	13.81	21.54	15.28	39.83
	28	11.7	12.96		

complex multi-phase system, the self-cleaning performance of hardened cement paste may not only be dominated by the additional structural or crystalline defects of the TiO_2-cement compound. In other words, for TiO_2-cement paste compound, a high photocatalytic activity doesn't guarantee a better de-colour performance. The surface conditions and microstructures of hardened cement paste samples can also influence the self-cleaning performance, which will be discussed in Section 3.4.

3.4. Microstructure of hardened cement paste

3.4.1. Specific surface area and pore size distribution

The specific surface area measured by the NAD method is shown in Table 6 with the BET interpretation. In Table 6, the specific surface area (SSA) of cement paste at 1 day decreases with the concentration of TiO_2, while at 28 days the SSA of paste increased with the concentration of TiO_2. At 28 days, the SSA in paste containing 0.05% and 0.10% TiO_2 reduces by 33.49% and 15.28% compared to that of 1 day, while in the reference paste the SSA reduces by 55.74%. Moreover, at 28 days, the adsorption average pore width in paste containing 0.05% and 0.10% TiO_2 reduces by 37.96% and 39.83%, while in the reference paste the adsorption average pore width reduces by 24.76%. As mentioned before, the SSA of TiO_2 xerogel is 244.75 m^2/g. It is obvious that at 28 days the increased values of SSA in hardened cement paste containing 0.05% and 0.10% TiO_2 are much greater than the pure growth caused by superposition of the SSA of nano TiO_2 particles and hardened paste. These results indicated that the presence of TiO_2 hydrosol in hardened cement paste could inhibit the decrease of SSA caused by cement hydration, which may be related to the change of morphology of hydration products and distribution of pores.

The cumulative pore size distribution (CPSD) and differential pore size distribution (DPSD) of the paste samples at 1d and 28 d are presented in Fig. 7. As can be seen from Fig. 7, after 1 day hydration, the pore volumes of gel micropores, mesopores and capillary pores [76] are higher than that of hardened cement paste containing TiO_2, and the pore volumes of pores reduced with the concentration of TiO_2. At 28 days, the pore volume of gel micropores in hardened cement paste containing 0.10% TiO_2 is the highest, and the pore volume of mesopores and capillary pores in hardened cement paste containing 0.01% is the highest. According to the results in [77], a higher volume of capillary porosity between 10 and 50 nm in mortars reveals a stronger photocatalytic activity. In Fig. 7(b), the volume of capillary porosity between 10 and 50 nm decreases obviously from 1 day to 28 days hydration, and the volumes of capillary porosity in that range of the cement paste containing 0.05% and 0.10% TiO_2 are similar while the volume of capillary porosity in that range of cement paste containing 0.01% TiO_2 is the lowest. These results of pore distribution can successfully explain the reduction of self-cleaning performance of TiO_2 modified cement paste at different hydration age, an earlier hydration age represents a larger volume of capillary porosity in the range of 10–50 nm and a higher value of SSA, which are helpful for the improvement of photocatalytic activity and self-cleaning performance of cement paste.

3.4.2. SEM analysis

The morphology of hardened cement paste modified with different concentration of TiO_2 hydrosol at 1 day and 28 days are presented in Figs. 8 and 9. From Fig. 8(a) and (b), it can be seen that the hydration product AFt in the reference sample and sample containing 0.01% TiO_2 is the typical needle-like shape with relatively uniform size [78,79], and the C-S-H is the dense gelatinous inner product [80]. While in the hardened cement paste containing 0.05% TiO_2, the AFt presents the shape of hexagonal prisms with shorted length. In Fig. 8(d) and (e), in the paste containing 0.10% TiO_2, the hexagonal prisms are tangled by wire like amorphous C-S-H gels [80], which are surrounding the C_3S grains. These images directly confirmed that the nucleation and formation of AFt at an early age are inhibited by the TiO_2 hydrosol.

In Fig. 9(a), after 28 days hydration, the main hydration products, like calcium hydroxide (CH), C-S-H gel and AFt, can be seen in the reference hardened cement paste, and the amount of AFt greatly reduces compared with that in Fig. 8(a). While, in the hardened cement paste containing 0.05% TiO_2 hydrosol (Fig. 9(b)), fibrous, radial crystal aggregates of AFt and petal shaped AFm are observed, and a number of small and short rod- shaped Ettringite crystals (Type 2 Ettringite crystals) [81] with about 3 μm length and 0.1 to 0.2 μm thickness are also observed. In the hardened cement paste containing 0.10% TiO_2 hydrosol (Fig. 9(c)), the clusters of AFt, AFm and C-S-H gel can be seen clearly, and the pores of hardened cement are filled with the areatus crystals.

The results of SEM images of hardened cement paste at 1 day and 28 days can explain the change of SSA caused by TiO_2 hydrosol. The amount and morphology of cement hydration products at 1 day and

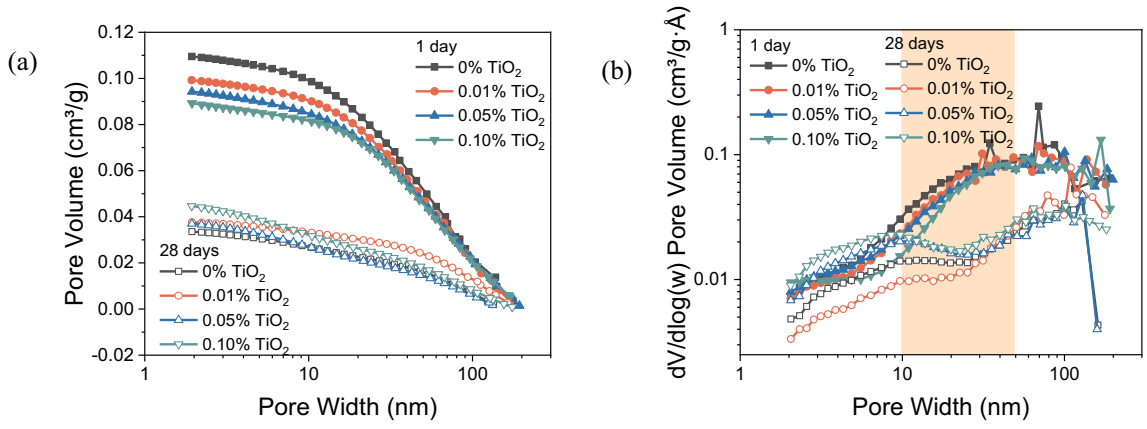

Fig. 7. Cumulative (a) and differential (b) pore size distributions of hardened cement paste at 1 d and 28 d.

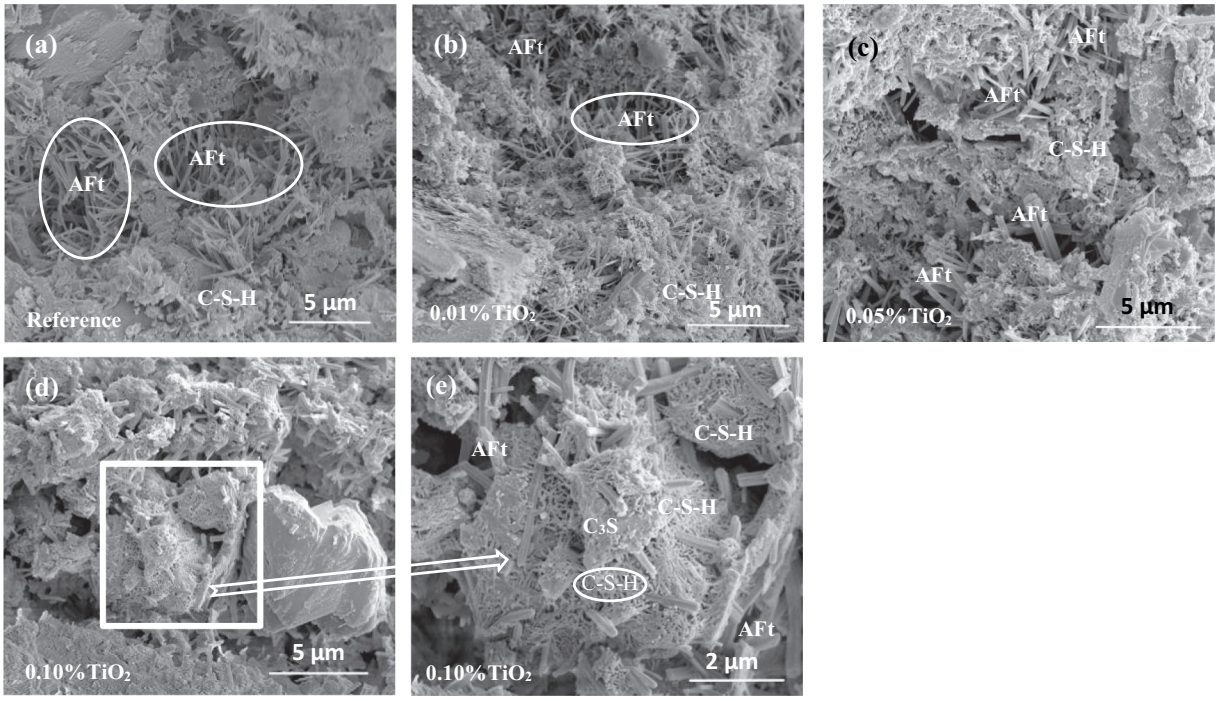

Fig. 8. SEM photos of hardened cement paste at 1 day (a. Reference; b. containing 0.01% TiO_2; c. containing 0.05% TiO_2; d. containing 0.10% TiO_2 magnified 15,000×; e. containing 0.10% TiO_2 magnified 35,000×).

28 days, like C-S-H and AFt, are impacted more by the concentration of TiO_2 hydrosol. At 1 day, the retardation of nucleation and formation of AFt and C-S-H led to the smaller SSA of hardened cement paste containing TiO_2 hydrosol. While at 28 days, the pores of hardened cement paste are filled with plenty of clusters of short barrel- shaped AFt, flake-like AFm and C-S-H gel, which led to a bigger SSA as compared with the reference paste.

4. Discussion

4.1. Dispersion of TiO_2 in hardened cement paste matrix

Agglomeration and coagulation are the main physicochemical processes restricting the photocatalytic activity of nanodispersed TiO_2 hydrosols or nano powders [82]. However, it is difficult to distinguish nano TiO_2 from cement by energy dispersive X- ray spectroscopy (EDX) element analysis, because the cement also contains titanium [83,84]. The confocal Raman microscope (CRM) is an ideal instrument for heterogeneous materials that show local fluorescence, which has been used to characterize the clinkers and hydration products of hardened cement paste [85–88]. Due to the non-destructive nature of the method, it can easily be applied to aqueous systems and both amorphous as well as crystalline components can be studied. Since TiO_2 is a typical crystalline compound, the distribution of nano TiO_2 crystals on the surface of the hardened cement paste can be observed by CRM more precisely and easily.

The average Raman spectra for hardened cement paste containing TiO_2 measured by CRM are shown in Fig. 10. The Raman bands at 144, 197 and 639 cm^{-1} are assigned to e_g modes, and the band at 144 cm^{-1} is very intense and sharp [89,90]. Raman spectroscopy can also be used to determine (approximately) the anatase content of impure rutile and other compounds [89]. As shown in Fig. 10, the Raman band of anatase TiO_2 at 144 cm^{-1} is more obvious in the hardened cement paste containing 0.05% and 0.10% TiO_2 hydrosol, while the wide Raman band of amorphous carbon [86] is clear in the reference paste and paste containing 0.01% TiO_2 paste. In hardened cement composites, the Raman spectrum of the ettringite is dominated by the Raman band around 1009 cm^{-1} and weaker band at 628 cm^{-1} [91,92], and the calcite ($CaCO_3$) is dominated by the narrow and intense Raman band at 1085 cm^{-1} [86,93–95] and weaker band at 711 cm^{-1} [86], the Raman modes of pure Portlandite ($Ca(OH)_2$) at 252 cm^{-1}, 356 cm^{-1} and approximate 680 cm^{-1} [96]. In Fig. 10, the peak intensity of Ettringite at 1000 cm^{-1} increased with the content of TiO_2 while the peak of calcite at 1085 cm^{-1} is observed in all samples. The wide peak in the range of

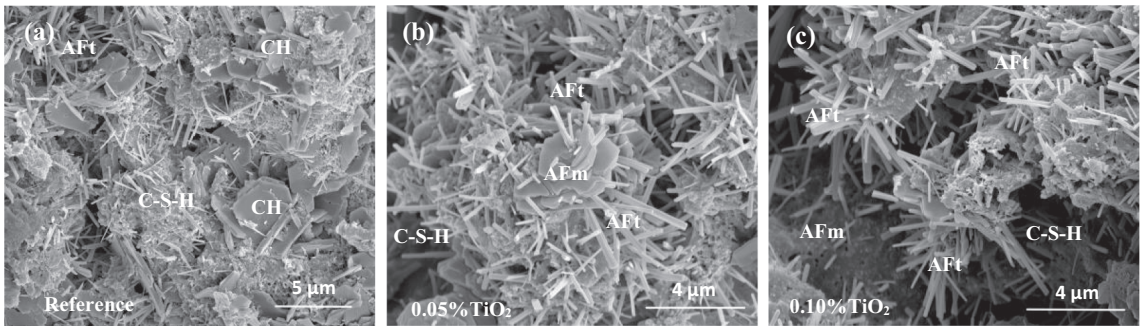

Fig. 9. SEM photos of cement paste at 28 days (a. Reference; b. containing 0.05% TiO_2; c. containing 0.10% TiO_2).

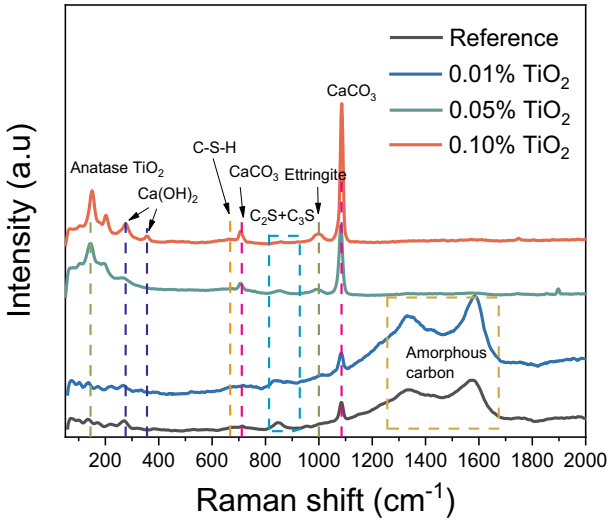

Fig. 10. Average Raman spectra of the different cements obtained by CRM (50–2000 cm^{-1} region).

800–900 cm^{-1} is referred to the unhydrated C_3S and C_2S [97]. As shown in Fig. 10, the peak intensity of unhydrated C_3S and C_2S is very weak on the surface of hardened cement paste with 0.05% and 0.10% TiO_2 hydrosol, indicating the more complete hydration of cement clinkers.

The Raman images of the anatase TiO_2 and the main hydration products spatial distributions in the hardened cement paste are shown in Fig. 11. The Raman band of 144 cm^{-1} [86], 356 cm^{-1} [96], 667 cm^{-1} [87], 839 cm^{-1} [97], 860 cm^{-1} [97], 1000 cm^{-1} [91,92] and 1085 cm^{-1} [86,93–95] are referred to the phase of anatase TiO_2, Portlandite, C-S-H, C_3S, C_2S, ettringite and calcite, respectively. In Fig. 11, in hardened cement paste containing 0.01% TiO_2, very little anatase TiO_2 is observed in the surface pores, while in the paste containing 0.05% and 0.10% TiO_2, more anatase TiO_2 is observed in the surface pores. In addition, the TiO_2 clusters are surrounded by the C-S-H and Ettringite, especially in the pore areas. Compared with paste containing 0.05% TiO_2, the distribution area of TiO_2 in paste containing 0.10% is bigger and the amounts of unhydrated C_3S and C_2S are smaller.

4.2. Self-cleaning mechanism analysis

It is clear that the degradation mechanisms of RB in cement paste caused by TiO_2 hydrosols are important in the understanding and optimisation of self-cleaning efficiencies. As reported previously [98], the degradation mechanism of RB caused by nano TiO_2 is proposed to happen by two phenomena, one being the de-ethylation process that has also been reported in other studies [44,99], and a second which is the degradation process of the chromophore structure. Several mechanisms for photoinduced self-cleaning of nano TiO_2 have been proposed, including (1) photoinduced surface vacancy generation [100]; (2) photoinduced reconstruction of surface hydroxyl groups [101,102]; and (3) light-induced removal of the carbonaceous layer on the surface of TiO_2 exposed to air [103]. The foundation of these theories is that the nano TiO_2 particles dispersed evenly on the surface of the matrix and the surfaces of the nano TiO_2 particles are exposured to the air and pollutants.

Many previous studies [70,104–106] prove that the higher concentration of oxygen vacancies or other defects result in the stronger photoactivity of nano TiO_2, which is usually used to explain the better air purification property of photocatalytic cement-based materials [37,107]. According to the calculation results of Band energy and Urbach energy shown in Table 5, the hardened cement paste containing 0.05% TiO_2 presents the highest photocatalytic activity, however, it does not present the best self-cleaning performance based on the test results in the Section 3.3.1. Therefore, a new interpretation of self-cleaning performance enhancement of TiO_2 hydrosol modified Portland cement paste is proposed here.

For cement paste modified by nanodispersed TiO_2 hydrosols, the high self-cleaning performance can be interprated from two parts. Firstly, the nanoscale dispersion of TiO_2 hydrosol is added in the mixing water in preparing cement paste, which means the nano TiO_2 particles can scatter much more evenly in the paste along with the water through mixing compared to the powder TiO_2 particles. The results of CRM analysis confirm that the anatase nano TiO_2 particles are dispersed evenly in the matrix of hardened cement paste. Secondly, there is a retardation effect of TiO_2 hydrosol on cement hydration at the acceleration and the deceleration stages. According to the XRD and TG analyses of hardened cement paste at different hydration ages, the presence of TiO_2 hydrosol does not affect the types of hydration products but affects the content of hydration products at early age. The retardation and nucleation effect of nano TiO_2 hydroosl on cement hydration leads to the obviously different morphology and distribution of hydration products (see the SEM and CRM analyses in Sections 3 and 4). As a result, the spectific surface area of the hardened cement paste at 28 day modified with greater TiO_2 hydrosol is much higher than that of the reference. The larger specific surface area of cement paste meant the more reaction surface area for TiO_2 to degrade the RB molecules on the surface of cement paste, indicating the better self-cleaning performance of cement paste.

Fig. 12 reveals the two routes to explain the self-cleaning mechanism of TiO_2 hydrosol modified cement paste, one is the additional surface defects causing smaller energy band gap and better photocatalytic activity (see Fig. 12 (a)), and another one is the surface electron capture effect of nano sized cement hydration products, like AFt

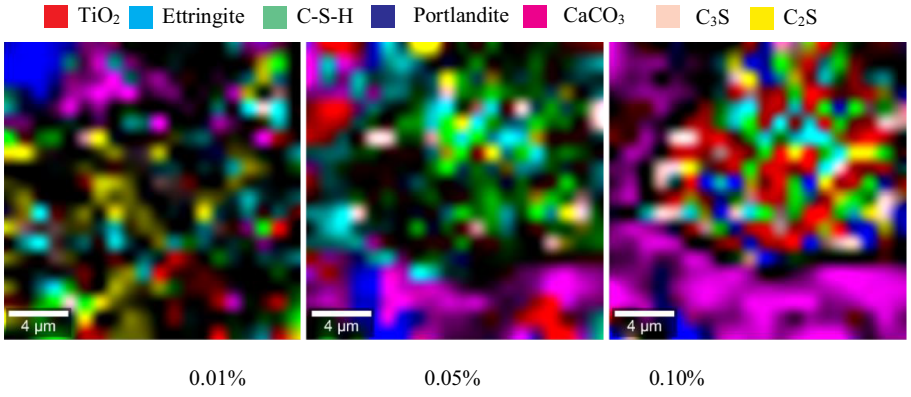

Fig. 11. Raman images by CRM of the evolution of the main phases present in paste containing different amount of TiO_2 at 28 days (the scan area is 20 μm × 20 μm).

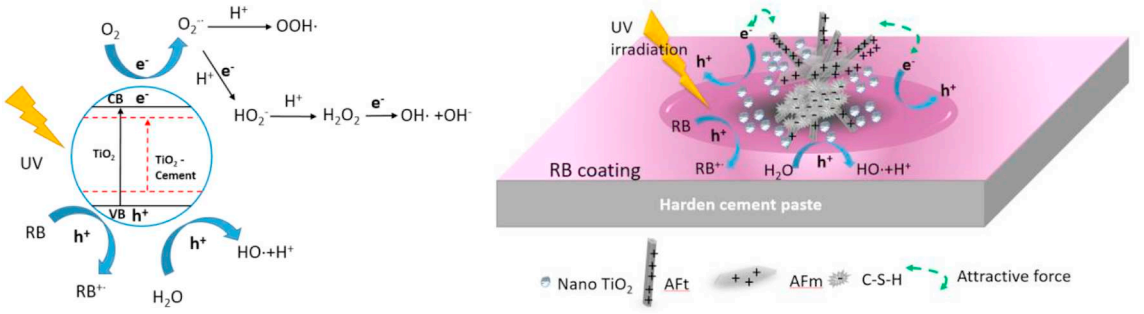

Fig. 12. Schematic diagram of self-cleaning mechanism of TiO_2 hydrosol modified photocatalytic cement paste.

and AFm phases (see Fig. 12 (b)). As mentioned in Section 3.3, the semiconductor electronic structure of TiO_2 can be disturbed by the hardened cement paste through the creation of defect levels. Moreover, the self-cleaning ability of a photocatalytic cementitious material is not only influenced by the photocatalytic activity, but also influenced by the conditions of the nano TiO_2 surface. As mentioned in Section 3.2.1, the surface of TiO_2 nano particles turns to negative at high pH system. In other words, in a cement-based environment, the TiO_2 particles tend to absorb on the surface of hydration phases with the positively charged surface, like AFt, AFm phases. The CRM images support that the non-agglomerated TiO_2 particles are surrounded by the positively charged AFt and AFm phases, which could be interpreted as that AFt and AFm can be the receptors of photo-induced electrons. When the electrons on the surface of TiO_2 are promoted by UV illumination, the electrons are trapped by positively charged AFt and AFm phases, which reduces the possibility of the electron-hole recombination. The surface electron capture effect is stronger at a larger concentration of TiO_2 hydrosol based on the results in Section 3.3.1. As a result, the tested TiO_2 modified cement paste shows a good self-cleaning performance.

From what has been discussed above, at low concentration of TiO_2 (< wt. 0.05% of cement), the self-cleaning performance of hardened cement paste is mainly dominated by the additional surface defects. While, at high concentration of TiO_2 (> wt. 0.10% of cement), the surface electron capture effects of cement hydration products predominate the efficiency of de-colour rate of hardened cement paste. Moreover, the enhancement of self-cleaning performance induced by the photocatalytic activity is much higher than that induced by the surface electron capture effect.

5. Conclusions

In this study, the influences of very low concentration nano dispersed TiO_2 hydrosol on the self-cleaning properties of hardened Portland cement paste (HPCP) are investigated on the cement hydration process and microstructure evolution. The following conclusions are drawn:

(1) Due the positively charged TiO_2 particles in hydrosol carrying functional group COOH, the cement hydration process is slightly retarded when mixing TiO_2 hydrosol in water at early age. The category of cement hydration products is unaffected but the microstructure of hardened cement paste is affected. The modified microstructure of hardened cement paste presented a bigger specific surface area at 28 days than that of the reference paste, and the specific surface area of paste increased with the concentration of TiO_2.

(2) The self-cleaning performance of modified HPCP is influenced by the higher optical photocatalytic activity of TiO_2-cement paste and the morphology of cement hydration products at different ages. At each test hydration age, the colour change rate in modified HPCP is increased with the concentration of TiO_2 hydrosol, but the increment is not proportional to the concentration of TiO_2 hydrosol. The colour change rate of modified HPCP with higher concentrations of TiO_2 (> 0.05% wt. of cement) decreases with the hydration age of cement.

(3) At lower TiO_2 hydrosol concentration (< 0.05% wt. of cement), the increase of additional surface defects of TiO_2 dominates the enhancement of self-cleaning performance of hardened cement paste. While in the higher concentration of TiO_2 hydrosol (> 0.05% wt. of cement), the contribution of the surface electron capture effect of hydration products to the enhancement of self-cleaning performance is larger. Under the UV irradiation, the recombination of electron-hole on the surface of nano TiO_2 can be resisted because the photo-induced electrons trapped by the positively charged AFt and AFm phase.

(4) A new mechanism of the self-cleaning performance enhancement of TiO_2 hydrosol modified hardened cement paste is proposed. The coupling of surface defects of nano TiO_2 particles and a surface electron capture effect generated by the special cluster structures of TiO_2 and main hydration products, like AFt, AFm and C-S-H are observed. Since the TiO_2 hydrosol affect the cement hydration at lower concentration, the lower-impacted HPCP creates more additional surface defects of TiO_2 particles. With the increase of TiO_2 hydrosol, the higher-impacted cement hydration products become the capturers of photo-induced electrons, which effect also improves the self-cleaning performance of HPCP.

CRediT authorship contribution statement

Zixiao Wang:Methodology, Investigation, Data curation, Formal analysis, Validation, Writing - original draft.**Qingliang Yu**:Conceptualization, Supervision, Project administration, Writing - review & editing.**Florent Gauvin**:Writing - review & editing.**Pan Feng**:Resources.**Ran Qianping**:Resources.**H.J.H. Brouwers**:Supervision, Writing - review & editing.

Declaration of competing interest

The authors declare that they have no known competing financial interests or personal relationships that could have appeared to influence the work reported in this paper.

Acknowledgement

The authors appreciate the financial supports from the National Natural Science Foundation of China (No. 1706222, No. 51708108), the China Scholarship Council (No. 201806090146) and Eindhoven

University of Technology (TU/e). The authors gratefully acknowledge M.Sc. Bin Meng (Building Performance group of TU/e) for his help in processing data of self-cleaning performance characterization, and Prof. Albert Schenning and M.Sc. Xinglong Pan (Stimuli-responsive Functional Materials & Devices group of TU/e) for their advices and comments in the measurements of the spectra analysis.

Appendix A. Supplementary data

Supplementary data to this article can be found online at https://doi.org/10.1016/j.cemconres.2020.106156.

References

[1] P. Berdahl, H. Akbari, L.S. Rose, Aging of reflective roofs: soot deposition, Appl. Opt. 41 (2002) 2355, https://doi.org/10.1364/AO.41.002355.
[2] M. Sleiman, T.W. Kirchstetter, P. Berdahl, H.E. Gilbert, S. Quelen, L. Marlot, C.V. Preble, S. Chen, A. Montalbano, O. Rosseler, H. Akbari, R. Levinson, H. Destaillats, Soiling of building envelope surfaces and its effect on solar reflectance - part II: development of an accelerated aging method for roofing materials, Sol. Energy Mater. Sol. Cells 122 (2014) 271–281, https://doi.org/10.1016/j.solmat.2013.11.028.
[3] Q.L. Yu, Y. Hendrix, S. Lorencik, H.J.H. Brouwers, Field study of NO_x degradation by a mineral-based air purifying paint, Build. Environ. 142 (2018) 70–82, https://doi.org/10.1016/j.buildenv.2018.06.014.
[4] M.M. Ballari, M. Hunger, G. Hüsken, H.J.H. Brouwers, NOx photocatalytic degradation employing concrete pavement containing titanium dioxide, Appl. Catal. B Environ. 95 (2010) 245–254, https://doi.org/10.1016/j.apcatb.2010.01.002.
[5] J. Chen, C. sun Poon, Photocatalytic construction and building materials: from fundamentals to applications, Build. Environ. 44 (2009) 1899–1906, https://doi.org/10.1016/j.buildenv.2009.01.002.
[6] Z. Abbas, J.P. Holmberg, A.K. Hellström, M. Hagström, J. Bergenholtz, M. Hassellöv, E. Ahlberg, Synthesis, characterization and particle size distribution of TiO_2 colloidal nanoparticles, Colloids Surfaces A Physicochem. Eng. Asp. 384 (2011) 254–261, https://doi.org/10.1016/j.colsurfa.2011.03.064.
[7] T. Liu, F. Li, X. Li, TiO_2 hydrosols with high activity for photocatalytic degradation of formaldehyde in a gaseous phase, J. Hazard. Mater. 152 (2008) 347–355, https://doi.org/10.1016/j.jhazmat.2007.07.003.
[8] E. Burunkaya, M. Akarsu, H. Erdem Çamurlu, Ö. Kesmez, Z. Yeşil, M. Asiltürk, E. Arpaç, Production of stable hydrosols of crystalline TiO_2 nanoparticles synthesized at relatively low temperatures in diverse media, Appl. Surf. Sci. 265 (2013) 317–323, https://doi.org/10.1016/j.apsusc.2012.11.003.
[9] P. Alphonse, A. Varghese, C. Tendero, Stable hydrosols for TiO_2 coatings, J. Sol-Gel Sci. Technol. 56 (2010) 250–263, https://doi.org/10.1007/s10971-010-2301-y.
[10] J.X. Yu, R.A. Chi, X.Z. Su, Z.Y. He, Y.F. Qi, Y.F. Zhang, Desorption behavior of methylene blue on pyromellitic dianhydride modified biosorbent by a novel eluent: acid TiO_2 hydrosol, J. Hazard. Mater. 177 (2010) 222–227, https://doi.org/10.1016/j.jhazmat.2009.12.021.
[11] A. Molea, V. Popescu, N.A. Rowson, A.M. Dinescu, Influence of pH on the formulation of TiO_2 nano-crystalline powders with high photocatalytic activity, Powder Technol. 253 (2014) 22–28, https://doi.org/10.1016/j.powtec.2013.10.040.
[12] B.P. Singh, S. Nayak, S. Samal, S. Bhattacharjee, L. Besra, The role of poly(methacrylic acid) conformation on dispersion behavior of nano TiO_2 powder, Appl. Surf. Sci. 258 (2012) 3524–3531, https://doi.org/10.1016/j.apsusc.2011.11.107.
[13] H.S. Bae, M.K. Lee, W.W. Kim, C.K. Rhee, Dispersion properties of TiO_2 nanopowder synthesized by homogeneous precipitation process at low temperatures, Colloids Surfaces A Physicochem. Eng. Asp. 220 (2003) 169–177, https://doi.org/10.1016/S0927-7757(03)00077-3.
[14] K. Bourikas, M. Stylidi, D.I. Kondarides, X.E. Verykios, Adsorption of acid Orange 7 on the surface of titanium dioxide, Langmuir 21 (2005) 9222–9230, https://doi.org/10.1021/la051434g.
[15] E. Ghenne, F. Dumont, C. Buess-Herman, Stability of TiO_2 hydrosols synthesized by hydrolysis of titanium tetraethoxide, Colloids Surfaces A Physicochem. Eng. Asp. 131 (1998) 63–67.
[16] O.B. Pavlova-Verevkina, Y.A. Shevchuk, V.V. Nazarov, Coagulation peculiarities and fractionation of nanodispersed titanium dioxide hydrosol, Colloid J. Russ. Acad. Sci. Kolloidn. Zhurnal. 65 (2003) 474–477, https://doi.org/10.1023/A:1025125019994.
[17] O.B. Pavlova-Verevkina, S.N. Chvalun, E.D. Politova, V.V. Nazarov, L.A. Ozerina, A.N. Ozerin, Study of the stable nanocrystalline TiO_2 hydrosol and its fractions, J. Sol-Gel Sci. Technol. 35 (2005) 91–97, https://doi.org/10.1007/s10971-005-1311-7.
[18] E. Santacesaria, M. Tonello, G. Storti, R.C. Pace, S. Carrà, Kinetics of titanium dioxide precipitation by thermal hydrolysis, J. Colloid Interface Sci. 111 (1986) 44–53, https://doi.org/10.1016/0021-9797(86)90005-6.
[19] Z. Wang, P. Feng, H. Chen, Q. Yu, Photocatalytic performance and dispersion stability of nanodispersed TiO_2 hydrosol in electrolyte solutions with different cations, J. Environ. Sci.. (n.d.). doi:https://doi.org/10.1016/j.jes.2019.07.013.
[20] S. Fazio, J. Guzm, M.T. Colomer, A. Salomoni, R. Moreno, Colloidal stability of nanosized titania aqueous suspensions, J. Eur. Ceram. Soc. 28 (2008) 2171–2176, https://doi.org/10.1016/j.jeurceramsoc.2008.02.017.
[21] P. Leroy, C. Tournassat, M. Bizi, Influence of surface conductivity on the apparent zeta potential of TiO_2 nanoparticles, J. Colloid Interface Sci. 356 (2011) 442–453, https://doi.org/10.1016/j.jcis.2016.01.075.
[22] O.B. Pavlova-Verevkina, L.A. Ozerina, V.V. Nazarov, N.M. Surin, Electrolyte-induced destabilization of hydrosols containing uniform TiO_2 nanoparticles, Colloid J 69 (2007) 492–497, https://doi.org/10.1134/S1061933X07040114.
[23] M.K. Ridley, V.A. Hackley, M.L. Machesky, I. State, W. Sur, G.D. V, Characterization and surface-reactivity of nanocrystalline anatase in aqueous solutions, Langmuir 22 (2006) (2006) 10972–10982, https://doi.org/10.1021/la061774h.
[24] J. Zhang, P. Jiang, P. Sun, Q. Wang, J. Kuang, W. Liu, W.-B. Cao, Role of ammonium ions on the stability of TiO_2 sol, J. Dispers. Sci. Technol. 2691 (2018) 1–6, https://doi.org/10.1080/01932691.2018.1472002.
[25] D. Marchon, R.J. Flatt, Mechanisms of cement hydration, Sci. Technol. Concr. Admixtures. 41 (2015) 129–145, https://doi.org/10.1016/B978-0-08-100693-1.00008-4.
[26] A.R. Jayapalan, B.Y. Lee, S.M. Fredrich, K.E. Kurtis, Influence of additions of anatase TiO_2 nanoparticles on early-age properties of cement-based materials, Transp. Res. Rec. J. Transp. Res. Board. 2141 (2010) 41–46, https://doi.org/10.3141/2141-08.
[27] B.Y. Lee, K.E. Kurtis, Influence of TiO_2 nanoparticles on early C_3S hydration, J. Am. Ceram. Soc. 93 (2010) 3399–3405, https://doi.org/10.1111/j.1551-2916.2010.03868.x.
[28] J. Chen, S.C. Kou, C.S. Poon, Hydration and properties of nano-TiO_2 blended cement composites, Cem. Concr. Compos. 34 (2012) 642–649, https://doi.org/10.1016/j.cemconcomp.2012.02.009.
[29] A.R. Jayapalan, M.L. Jue, K.E. Kurtis, Nanoparticles and apparent activation energy of Portland cement, J. Am. Ceram. Soc. 97 (2014) 1534–1542, https://doi.org/10.1111/jace.12878.
[30] R. Zhang, X. Cheng, P. Hou, Z. Ye, Influences of nano-TiO_2 on the properties of cement-based materials: hydration and drying shrinkage, Constr. Build. Mater. 81 (2015) 35–41, https://doi.org/10.1016/j.conbuildmat.2015.02.003.
[31] A.P. Werle, M.L. De Souza, K. Loh, R. Ando, V.M. John, The performance of a self-cleaning cool cementitious surface, Energy Build 114 (2016) 200–205, https://doi.org/10.1016/j.enbuild.2015.06.025.
[32] M. Janus, J. Zatorska, A. Czyzewski, K. Bubacz, E. Kusiak-Nejman, A.W. Morawski, Self-cleaning properties of cement plates loaded with N,C-modified TiO_2 photocatalysts, Appl. Surf. Sci. 330 (2015) 200–206, https://doi.org/10.1016/j.apsusc.2014.12.113.
[33] A. Zhao, J. Yang, E.H. Yang, Self-cleaning engineered cementitious composites, Cem. Concr. Compos. 64 (2015) 74–83, https://doi.org/10.1016/j.cemconcomp.2015.09.007.
[34] M.V. Diamanti, B. Del Curto, M. Ormellese, M.P. Pedeferri, Photocatalytic and self-cleaning activity of colored mortars containing TiO_2, Constr. Build. Mater. 46 (2013) 167–174, https://doi.org/10.1016/j.conbuildmat.2013.04.038.
[35] M.V. Diamanti, R. Paolini, M. Rossini, A.B. Aslan, M. Zinzi, T. Poli, M.P. Pedeferri, Long term self-cleaning and photocatalytic performance of anatase added mortars exposed to the urban environment, Constr. Build. Mater. 96 (2015) 270–278, https://doi.org/10.1016/j.conbuildmat.2015.08.028.
[36] R. Khataee, V. Heydari, L. Moradkhannejhad, M. Safarpour, S.W. Joo, Self-cleaning and mechanical properties of modified white cement with nanostructured TiO_2, J. Nanosci. Nanotechnol. 13 (2013) 5109–5114, https://doi.org/10.1166/jnn.2013.7586.
[37] A. Folli, C. Pade, T.B. Hansen, T. De Marco, D.E. MacPhee, TiO_2 photocatalysis in cementitious systems: insights into self-cleaning and depollution chemistry, Cem. Concr. Res. 42 (2012) 539–548, https://doi.org/10.1016/j.cemconres.2011.12.001.
[38] X. Ding, S. Pan, C. Lu, H. Guan, X. Yu, Y. Tong, Hydrophobic photocatalytic composite coatings based on nano-TiO_2 hydrosol and aminopropyl terminated polydimethylsiloxane prepared by a facile approach, Mater. Lett. 228 (2018) 5–8, https://doi.org/10.1016/j.matlet.2018.05.103.
[39] E. Jimenez-Relinque, I. Llorente, M. Castellote, TiO_2 cement-based materials: understanding optical properties and electronic band structure of complex matrices, Catal. Today 287 (2017) 203–209, https://doi.org/10.1016/j.cattod.2016.11.015.
[40] E. Jimenez-Relinque, J.R. Rodriguez-Garcia, A. Castillo, M. Castellote, Characteristics and efficiency of photocatalytic cementitious materials: type of binder, roughness and microstructure, Cem. Concr. Res. 71 (2015) 124–131, https://doi.org/10.1016/j.cemconres.2015.02.003.
[41] E. Cerro-Prada, M. Manso, V. Torres, J. Soriano, Microstructural and photocatalytic characterization of cement-paste sol-gel synthesized titanium dioxide, Front. Struct. Civ. Eng. 10 (2016) 189–197, https://doi.org/10.1007/s11709-015-0326-6.
[42] L. Yang, A. Hakki, F. Wang, D.E. Macphee, Photocatalyst efficiencies in concrete technology: the effect of photocatalyst placement, Appl. Catal. B Environ. 222 (2018) 200–208, https://doi.org/10.1016/j.apcatb.2017.10.013.
[43] Z. Wang, P. Feng, H. Chen, Q. Yu, Photocatalytic performance and dispersion stability of nanodispersed TiO_2 hydrosol in electrolyte solutions with different cations, J. Environ. Sci. 88 (2020) 59–71, https://doi.org/10.1016/j.jes.2019.07.013.
[44] P. Qu, J. Zhao, T. Shen, H. Hidaka, TiO_2-assisted photodegradation of dyes: a study of two competitive primary processes in the degradation of RB in an aqueous TiO_2 colloidal solution, J. Mol. Catal. A Chem. 129 (1998) 257–268, https://doi.org/10.1016/S1381-1169(97)00185-4.

[45] T. Watanabe, T. Takizawa, K. Honda, Photocatalysis through excitation of adsorbates. 1. Highly efficient N-deethylation of rhodamine B adsorbed to CdS, J. Phys. Chem. 81 (1977) 1845–1851, https://doi.org/10.1021/j100534a012.

[46] E. Jimenez-Relinque, J.R. Rodriguez-Garcia, A. Castillo, M. Castellote, Characteristics and efficiency of photocatalytic cementitious materials: type of binder, roughness and microstructure, Cem. Concr. Res. 71 (2015) 124–131, https://doi.org/10.1016/j.cemconres.2015.02.003.

[47] H. Suk, Y. Mu, J. Won, Y. Kyong, J. Kook, D. Cho, Characterization of bioactive RGD peptide immobilized onto poly (acrylic acid) thin films by plasma polymerization, Appl. Surf. Sci. 257 (2010) 596–602, https://doi.org/10.1016/j.apsusc.2010.07.040.

[48] E. Portenkirchner, G. Neri, J. Lichtinger, J. Brumbarov, C. Rüdiger, R. Gernhäuser, J. Kunze-Liebhäuser, Tracking areal lithium densities from neutron activation – quantitative Li determination in self-organized TiO_2 nanotube anode materials for Li-ion batteries, Phys. Chem. Chem. Phys. (2017), https://doi.org/10.1039/c7cp00180k.

[49] M.R. Ayers, A.J. Hunt, Titanium oxide aerogels prepared from titanium metal and hydrogen peroxide, Mater. Lett. 34 (1998) 290–293.

[50] V. Etacheri, M.K. Seery, S.J. Hinder, S.C. Pillai, Oxygen rich Titania: a dopant free, high temperature stable, and visible-light active anatase photocatalyst, Adv. Funct. Mater. 21 (2011) 3744–3752, https://doi.org/10.1002/adfm.201100301.

[51] J.A. Davis, R.O. James, J.O. Leckie, Surface ionization and complexation at the oxide/water interface I. computation of electrical double layer properties in simple electrolytes, J. Colloid Interface Sci. 63 (1977) 480–499, https://doi.org/10.1016/S0021-9797(78)80009-5.

[52] S. Liufu, H. Xiao, Y. Li, Adsorption of poly(acrylic acid) onto the surface of titanium dioxide and the colloidal stability of aqueous suspension, J. Colloid Interface Sci. 281 (2005) 155–163, https://doi.org/10.1016/j.jcis.2004.08.075.

[53] Y.R. Zhang, X.M. Kong, Z.B. Lu, Z.C. Lu, S.S. Hou, Effects of the charge characteristics of polycarboxylate superplasticizers on the adsorption and the retardation in cement pastes, Cem. Concr. Res. 67 (2015) 184–196, https://doi.org/10.1016/j.cemconres.2014.10.004.

[54] R.H. Rogue, W. Lerch, Hydration of Portland cement compounds, Ind. Eng. Chem. Res. 26 (1934) 837–847, https://doi.org/10.1021/ie50296a007.

[55] K.L. Scrivener, P. Juilland, P.J.M. Monteiro, Advances in understanding hydration of Portland cement, Cem. Concr. Res. 78 (2015) 38–56, https://doi.org/10.1016/j.cemconres.2015.05.025.

[56] K.L. Scrivener, A. Nonat, Hydration of cementitious materials, present and future, Cem. Concr. Res. 41 (2011) 651–665, https://doi.org/10.1016/j.cemconres.2011.03.026.

[57] J. Cheung, A. Jeknavorian, L. Roberts, D. Silva, Impact of admixtures on the hydration kinetics of Portland cement, Cem. Concr. Res. 41 (2011) 1289–1309, https://doi.org/10.1016/j.cemconres.2011.03.005.

[58] J.P. Holmberg, E. Ahlberg, J. Bergenholtz, M. Hassellöv, Z. Abbas, Surface charge and interfacial potential of titanium dioxide nanoparticles: experimental and theoretical investigations, J. Colloid Interface Sci. 407 (2013) 168–176, https://doi.org/10.1016/j.jcis.2013.06.015.

[59] Z. Lu, X. Kong, C. Zhang, Y. Cai, Effect of highly carboxylated colloidal polymers on cement hydration and interactions with calcium ions, Cem. Concr. Res. 113 (2018) 140–153, https://doi.org/10.1016/j.cemconres.2018.08.010.

[60] F.R. Kong, L.S. Pan, C.M. Wang, D. La Zhang, N. Xu, Effects of polycarboxylate superplasticizers with different molecular structure on the hydration behavior of cement paste, Constr. Build. Mater. 105 (2016) 545–553, https://doi.org/10.1016/j.conbuildmat.2015.12.178.

[61] S. Tsivilis, G. Kakali, E. Chaniotakis, A. Souvaridou, A study on the hydration of Portland limestone cement by means of TG, J. Therm. Anal. Calorim. 52 (1998) 863–870, https://doi.org/10.1023/A:1010139312958.

[62] G. Kakali, S. Tsivilis, A. Tsialtas, Hydration of ordinary Portland cements made from raw mix containing transition element oxides, Cem. Concr. Res. 28 (1998) 335–340.

[63] I. Pane, W. Hansen, Investigation of blended cement hydration by isothermal calorimetry and thermal analysis, Cem. Concr. Res. 35 (2005) 1155–1164, https://doi.org/10.1016/j.cemconres.2004.10.027.

[64] N. De Belie, J. Kratky, S. Van Vlierberghe, Influence of pozzolans and slag on the microstructure of partially carbonated cement paste by means of water vapour and nitrogen sorption experiments and BET calculations, Cem. Concr. Res. 40 (2010) 1723–1733, https://doi.org/10.1016/j.cemconres.2010.08.014.

[65] D.S. Klimesch, A. Ray, The use of DTA/TGA to study the effects of ground quartz with different surface areas in autoclaved cement: quartz pastes. Part 1: a method for evaluating DTA/TGA results, Thermochim. Acta 289 (1996) 41–54, https://doi.org/10.1016/S0040-6031(96)03033-X.

[66] M. Asilturk, F. Sayılkan, S. Erdemoglu, M. Akarsu, H. Sayılkan, M. Erdemoglu, E. Arpac, Characterization of the hydrothermally synthesized nano-TiO_2 crystallite and the photocatalytic degradation of Rhodamine B, J. Hazard. Mater. B 129 (2006) 164–170, https://doi.org/10.1016/j.jhazmat.2005.08.027.

[67] T. Aarthi, G. Madras, Photocatalytic degradation of rhodamine dyes with nano-TiO_2, Ind. Eng. Chem. Res. 46 (2007) 7–14, https://doi.org/10.1021/ie060948n.

[68] A. Folli, U.H. Jakobsen, G.L. Guerrini, D.E. Macphee, Rhodamine B discolouration on TiO_2 in the cement environment: a look at fundamental aspects of the self-cleaning effect in concretes, J. Adv. Oxid. Technol. 12 (2009) 126–133, https://doi.org/10.1515/jaots-2009-0116.

[69] V. Nadtochenko, N. Denisov, A. Gorenberg, Y. Kozlov, P. Chubukov, J.A. Rengifo, C. Pulgarin, J. Kiwi, Correlations for photocatalytic activity and spectral features of the absorption band edge of TiO_2 modified by thiourea, Appl. Catal. B Environ. 91 (2009) 460–469, https://doi.org/10.1016/j.apcatb.2009.06.015.

[70] R. López, R. Gómez, Band-gap energy estimation from diffuse reflectance measurements on sol-gel and commercial TiO_2: a comparative study, J. Sol-Gel Sci. Technol. 61 (2012) 1–7, https://doi.org/10.1007/s10971-011-2582-9.

[71] M. Radecka, M. Rekas, A. Trenczek-Zajac, K. Zakrzewska, Importance of the band gap energy and flat band potential for application of modified TiO_2 photoanodes in water photolysis, J. Power Sources 181 (2008) 46–55, https://doi.org/10.1016/j.jpowsour.2007.10.082.

[72] S. Karapati, T. Giannakopoulou, N. Todorova, N. Boukos, S. Antiohos, D. Papageorgiou, E. Chaniotakis, D. Dimotikali, C. Trapalis, TiO_2 functionalization for efficient NO_x removal in photoactive cement, Appl. Surf. Sci. 319 (2014) 29–36, https://doi.org/10.1016/j.apsusc.2014.07.162.

[73] R. Bhatt, I. Bhaumik, S. Ganesamoorthy, A.K. Karnal, M.K. Swami, H.S. Patel, P.K. Gupta, Urbach tail and bandgap analysis in near stoichiometric $LiNbO_3$ crystals, Phys. Status Solidi Appl. Mater. Sci. 209 (2012) 176–180, https://doi.org/10.1002/pssa.201127361.

[74] D.C. Cronemeyer, Electrical and optical properties of rutile single crystals, Phys. Rev. 87 (1952) 876–886, https://doi.org/10.1103/PhysRev.87.876.

[75] Franz Urbach, The long-wavelength edge of photographic sensitivity and of the electronic absorption of solids, Phys. Rev. 92 (1953) 1324.

[76] P.K. Mehta, P.J.M. Monteiro, Concrete: Microsturcture, Properties and Materials, Third Edit, The McGraw-Hill Companies, Inc. All, 2006, https://doi.org/10.1036/0071462899.

[77] A.M. Kaja, H.J.H. Brouwers, Q.L. Yu, NO_x degradation by photocatalytic mortars: the underlying role of the CH and C-S-H carbonation, Cem. Concr. Res. 125 (2019) 105805, , https://doi.org/10.1016/j.cemconres.2019.105805.

[78] F. Goetz-Neunhoeffer, J. Neubauer, P. Schwesig, Mineralogical characteristics of Ettringites synthesized from solutions and suspensions, Cem. Concr. Res. 36 (2006) 65–70, https://doi.org/10.1016/j.cemconres.2004.04.037.

[79] E. Sakai, Y. Nikaido, T. Itoh, M. Daimon, Ettringite formation and microstructure of rapid hardening cement, Cem. Concr. Res. 34 (2004) 1669–1673, https://doi.org/10.1016/j.cemconres.2004.04.021.

[80] H.M. Jennings, B.J. Dalgleish, P.L. Pratt, Morphological development of hydrating tricalcium silicate as examined by electron microscopy techniques, J. Am. Ceram. Soc. 64 (1981) 567–572, https://doi.org/10.1111/j.1151-2916.1981.tb10219.x.

[81] P.K. Mehta, Mechanism of sulfate attack on Portland cement concrete- another look, Cem. Concr. Res. 13 (1983) 401–406.

[82] A. Brunelli, G. Pojana, S. Callegaro, A. Marcomini, Agglomeration and sedimentation of titanium dioxide nanoparticles (n-TiO_2) in synthetic and real waters, J. Nanopart. Res. 15 (2013), https://doi.org/10.1007/s11051-013-1684-4.

[83] J.. Potgieter, K.. Horne, S.. Potgieter, W. Wirth, An evaluation of the incorporation of a titanium dioxide producer's waste material in Portland cement clinker, Mater. Lett. 57 (2002) 157–163, https://doi.org/10.1016/s0167-577x(02)00723-1.

[84] D. Shang, M. Wang, Z. Xia, S. Hu, F. Wang, Incorporation mechanism of titanium in Portland cement clinker and its effects on hydration properties, Constr. Build. Mater. 146 (2017) 344–349, https://doi.org/10.1016/j.conbuildmat.2017.03.129.

[85] O. Mikhailova, A. del Campo, P. Rovnanik, J.F. Fernández, M. Torres-Carrasco, In situ characterization of main reaction products in alkali-activated slag materials by Confocal Raman Microscopy, Cem. Concr. Compos. 99 (2019) 32–39, https://doi.org/10.1016/j.cemconcomp.2019.02.004.

[86] M. Torres-Carrasco, A. del Campo, M.A. de la Rubia, E. Reyes, A. Moragues, J.F. Fernández, New insights in weathering analysis of anhydrous cements by using high spectral and spatial resolution Confocal Raman Microscopy, Cem. Concr. Res. 100 (2017) 119–128, https://doi.org/10.1016/j.cemconres.2017.06.003.

[87] J. Higl, M. Köhler, M. Lindén, Confocal Raman microscopy as a non-destructive tool to study microstructure of hydrating cementitious materials, Cem. Concr. Res. 88 (2016) 136–143, https://doi.org/10.1016/j.cemconres.2016.07.005.

[88] F. Liu, Z. Sun, Chemical mapping of cement pastes by using confocal Raman spectroscopy, Front. Struct. Civ. Eng. 10 (2016) 168–173, https://doi.org/10.1007/s11709-015-0323-9.

[89] I.R. Beattie, T.R. Gilson, Single crystal laser Raman spectroscopy, Proc. R. Soc. A, Math. Phys. Eng. Sci. 307 (1968) 407–429, https://doi.org/10.1098/rspa.1968.0199.

[90] T. Ohsaka, F. Izumi, Y. Fujiki, Raman spectrum of anatase, TiO_2, J. Raman Spectrosc. 7 (1978) 321–324, https://doi.org/10.1002/jrs.1250070606.

[91] L. Black, C. Breen, J. Yarwood, C.S. Deng, J. Phipps, G. Maitland, Hydration of tricalcium aluminate (C_3A) in the presence and absence of gypsum - studied by Raman spectroscopy and X-ray diffraction, J. Mater. Chem. 16 (2006) 1263–1272, https://doi.org/10.1039/b509904h.

[92] G. Renaudin, R. Segni, D. Mentel, J.-M. Nedelec, F. Leroux, C. Taviot-Gueho, A Raman study of the sulfated cement hydrates: ettringite and monosulfoaluminate, J. Adv. Concr. Technol. 5 (2007) 299–312, https://doi.org/10.3151/jact.5.299.

[93] S. Gunasekaran, G. Anbalagan, S. Pandi, Raman and infrared spectra of carbonates of calcite structure, J. Raman Spectrosc. 37 (2006) 892–899, https://doi.org/10.1002/jrs.1518.

[94] R. Masmoudi, K. Kupwade-Patil, A. Bumajdad, O. Büyüköztürk, In situ Raman studies on cement paste prepared with natural pozzolanic volcanic ash and ordinary Portland cement, Constr. Build. Mater. 148 (2017) 444–454, https://doi.org/10.1016/j.conbuildmat.2017.05.016.

[95] F. Liu, Z. Sun, C. Qi, Raman spectroscopy study on the hydration behaviors of Portland cement pastes during setting, J. Mater. Civ. Eng. 27 (2014) 04014223, , https://doi.org/10.1061/(asce)mt.1943-5533.0001189.

[96] T. Schmida, P. Dariz, Shedding light onto the spectra of lime: Raman and luminescence bands of CaO, $Ca(OH)_2$ and $CaCO_3$, J. Raman Spectrosc. 46 (2015) 141–146, https://doi.org/10.1002/jrs.4622.

[97] L. Black, Raman spectroscopy of cementitious materials, in: J. Yarwood,

R. Douthwaite, S.B. Duckett (Eds.), Spectrosc. Prop. Inorg. Organomet. Compd, 40 The Royal Society of Chemistry, Cambridge, 2009, pp. 72–127, , https://doi.org/10.1039/b715000h.

[98] S. Ortelli, M. Blosi, S. Albonetti, A. Vaccari, M. Dondi, A.L. Costa, TiO_2 based nano-photocatalysis immobilized on cellulose substrates, J. Photochem. Photobiol. A Chem. 276 (2014) 58–64, https://doi.org/10.1016/j.jphotochem.2013.11.013.

[99] T. Wu, G. Liu, J. Zhao, H. Hidaka, N. Serpone, Photoassisted degradation of dye pollutants. V. Self-photosensitized oxidative transformation of Rhodamine B under visible light irradiation in aqueous TiO_2 dispersions, J. Phys. Chem. B 102 (1998) 5845–5851, https://doi.org/10.1021/jp980922c.

[100] R. Wang, K. Hashimoto, A. Fujishima, M. Chikuni, E. Kojima, A. Kitamura, M. Shimohigoshi, T. Watanabe, Photogeneration of highly amphiphilic TiO_2 surfaces, Adv. Mater. 10 (1998) 135–138, https://doi.org/10.1002/(SICI)1521-4095(199801)10:2<135::AID-ADMA135>3.0.CO;2-M.

[101] N. Sakai, A. Fujishima, T. Watanabe, K. Hashimoto, Quantitative evaluation of the photoinduced hydrophilic conversion properties of TiO_2 thin film surfaces by the reciprocal of contact angle, J. Phys. Chem. B 107 (2003) 1028–1035, https://doi.org/10.1021/jp022105p.

[102] N. Sakai, A. Fujishima, T. Watanabe, K. Hashimoto, Enhancement of the photo-induced hydrophilic conversion rate of TiO_2 film electrode surfaces by anodic polarization, J. Phys. Chem. B 105 (2001) 3023–3026, https://doi.org/10.1021/jp003212r.

[103] T. Zubkoy, D. Stahl, T.L. Thompson, D. Panayotov, O. Diwald, J.T. Yates, Ultraviolet light-induced hydrophilicity effect on TiO_2(110) (1 × 1). Dominant role of the photooxidation of adsorbed hydrocarbons causing wetting by water droplets, J. Phys. Chem. B 109 (2005) 15454–15462, https://doi.org/10.1021/jp058101c.

[104] S.H. Elder, F.M. Cot, Y. Su, S.M. Heald, A.M. Tyryshkin, M.K. Bowman, Y. Gao, A.G. Joly, M.L. Balmer, A.C. Kolwaite, K.A. Magrini, D.M. Blake, The discovery and study of nanocrystalline TiO_2 -(MoO_3) core-shelf materials, J. Am. Chem. Soc. 122 (2000) 5138–5146, https://doi.org/10.1021/ja992768t.

[105] B. Choudhury, A. Choudhury, Oxygen defect dependent variation of band gap, Urbach energy and luminescence property of anatase, anatase-rutile mixed phase and of rutile phases of TiO_2 nanoparticles, Phys. E Low-Dimensional Syst. Nanostructures. 56 (2014) 364–371, https://doi.org/10.1016/j.physe.2013.10.014.

[106] M.M. Khan, S.A. Ansari, D. Pradhan, M.O. Ansari, D.H. Han, J. Lee, M.H. Cho, Band gap engineered TiO_2 nanoparticles for visible light induced photoelectrochemical and photocatalytic studies, J. Mater. Chem. A 2 (2014) 637–644, https://doi.org/10.1039/c3ta14052k.

[107] M.M. Ballari, Q.L. Yu, H.J.H. Brouwers, Experimental study of the NO and NO_2 degradation by photocatalytically active concrete, Catal. Today 161 (2011) 175–180, https://doi.org/10.1016/j.cattod.2010.09.028.